Mathl Modelling, Vol. 9, No. 2, pp. 125–145, 1987
Printed in Great Britain.

0270-0255/87 $3.00 + 0.00

A MODEL OF GLOBAL AND BASIN-SCALE ANOXIA

J. R. SOUTHAM, W. H. PETERSON and G. W. BRASS
Rosenstiel School of Marine and Atmospheric Science, University of Miami, Miami, FL 33149, U.S.A.

(*Received* 10 *December* 1986)

Communicated by J. J. O'Brien

Abstract—A simple steady-state 1-D model of the oceanic particulate organic carbon, dissolved oxygen and dissolved phosphate system has been developed to study global and basin-scale anoxia. The model has been calibrated with present-day data and yields estimates of the present-day new-carbon flux (0.65 mol C/yr m^2) and riverine phosphate flux (0.43 × 10^{-4} mol P/yr m^2). The model requires substantial departures from present-day conditions for the existence of global steady-state anoxia. Fertility well above present-day values is required (for present-day continental configurations) even with a substantial reduction in thermohaline circulation rates or ventilation. It is shown that small basins, such as the mid-Cretaceous North and South Atlantic, may attain steady-state anoxia with global fertility no greater than present-day values. Finally, it is suggested that large-scale anoxic events may be intrinsically transient phenomena and that modeling of the anoxic events recorded in the geologic record requires a 2-D time-dependent model.

1. INTRODUCTION

Examination of cores recovered by the Deep Sea Drilling Project has documented the worldwide existence of layers of black, organic-carbon-rich (1–30%) deep-sea sediments deposited during the upper Jurassic to the mid-Cretaceous [1–4]. The deposition of organic-rich sediments has been attributed to oceanic anoxic events of basin-wide and possibly global extent [5]. The origins of mid-Cretaceous black shales are important because these deposits represent a major source for the world petroleum production [6]. Episodes of widespread anoxia also occurred during earlier periods, including parts of the Ordivician, Silurian and Devonian.

Thierstein [7], in an overview of Mesozoic paleoceanography, identifies mid-Cretaceous oceanic anoxic events as one of the two most interesting topics of Mesozoic paleoceanography. The variety in the characteristics of organic sediments indicates multiple possible scenarios for anoxic events and has resulted in a variety of explanations for their occurrence. Some investigators have suggested that large-scale anoxic episodes are due to increased fertility resulting in the expansion of the oxygen minimum. This provides a particularly attractive explanation for the deposition of organic-rich sediments at intermediate depths. Stagnation, or at least a much weaker thermohaline circulation than at present and hence a reduced supply of oxygen to the abyssal waters has also been suggested. Finally, we suggested that a reduced flux of oxygen due to bottom water formation, because of the reduced solubility of oxygen in warm salty bottom water (WSBW) could lead to anoxia without requiring a more sluggish thermohaline circulation than that of today [8].

2. PROCESSES AND THEIR PARAMETERIZATION

Anoxia occurs whenever the oxygen consumption rate exceeds the oxygen supply rate. Anoxia involves the interaction of biological, chemical and physical transport processes. Hence the situation is sufficiently complex to require a quantitative study to determine the dominant processes and balances. With any mathematical model of a natural system many assumptions and simplifications are necessary to produce a tractable problem. It was our intent to include the minimum number of processes necessary for the existence of large-scale steady-state anoxia. The minimal model capable of describing global and/or basin-wide anoxia requires the following processes: (1) adequate representation of the physical transport processes; (2) supply of oxygen across the air–sea interface; and (3) production of new carbon in the euphotic zone with the subsequent sinking of organic particles into the deep ocean and oxidation of these sinking particles with the consumption of oxygen and the simultaneous release of nutrients. How we choose to represent these processes in the model will be discussed in sequence below (see Fig. 1 for a schematic sketch of the model).

2.1. Physical transport processes

Chemical cycles are essentially forced by fluxes into and out of the top and bottom of the ocean. Therefore, as Broecker and Peng [9] show, simple vertical models (in their work a simple two-box model) are useful in quantitatively understanding the primary features of marine chemical cycles. However, consideration of anoxia compels us to include more vertical structure than provided by simple box models. Taking the next step in complexity we have employed a surface reservoir interacting with a deep reservoir with continuous vertical structure. This is imperative because the portion of the domain that becomes anoxic is a model result and cannot be predicted *a priori*.

2.2. Supply of oxygen

The supply of oxygen across the air–sea interface is modeled by the interaction of a surface reservoir with an infinite atmosphere so that the oxygen content in the surface layer is maintained at essentially saturation.

2.3. Production oxidation of settling organic particles in the deep reservoir

The essential link between biological productivity and the deep ocean is the rain of organic particles from the surface layer. Nutrients are recycled many times in the surface layer, however, a small portion leaves the surface layer as particles. These particles sink with a settling velocity that is determined by the balance of hydrodynamic drag and gravity. The salient point is that their settling velocity ($\sim 10^2$ m/day) is many orders of magnitude greater than any estimate of the abyssal upwelling velocity. The settling particles are oxidized by bacteria and higher organisms which consume oxygen and release nutrients. At very low oxygen concentrations denitrification and nitrate reduction continue to oxidize the settling particles past the point of apparent oxygen exhaustion. Further carbon oxidation continues by means of anaerobic sulfate reduction. These processes are a consequence of anoxia, *not a cause*, and hence, not essential to a first-order theory of anoxia. Thus, for reasons of tractability, we will make the rather drastic assumption that oxidation of carbon ceases when the oxygen concentration goes to zero and ignore nitrate and sulfate consumption. We further assume that oxidation is first order in organic carbon and independent of oxygen until the oxygen concentration reaches zero at which point oxidation ceases. Although the bulk of the particle flux is oxidized in the water column some small portion of it is deposited on the bottom. Because we have neglected both nitrate and sulfate consumption we most

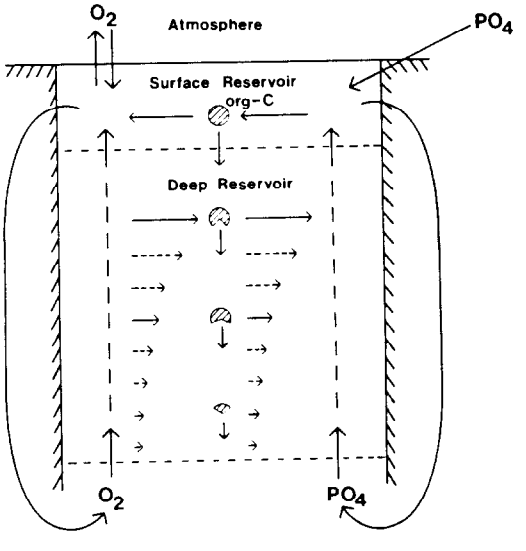

Fig. 1. Schematic sketch of the model which consists of a surface reservoir and an advective–diffusive deep reservoir. The surface reservoir exchanges oxygen with an infinite atmosphere and with the deep reservoir. Phosphate is added to the surface reservoir by river input and exchange with the deep reservoir. The surface reservoir is taken to the euphotic zone within which biological productivity produces a rain of organic particles that are oxidized in the deep layer consuming oxygen and releasing phosphate. Oxygen and phosphate are supplied to the bottom of the deep reservoir by deep water formation.

certainly, under anoxic conditions, overestimate the carbon flux to the sediments and underestimate the phosphate concentration in the deep.

3. MODEL DESCRIPTION AND EQUATIONS

3.1. Model description

The model, which is steady state, consists of a surface reservoir that interacts with a 1-D, advective and diffusive deep reservoir. Conservation equations for labile particulate organic carbon, dissolved oxygen and dissolved phosphate (henceforth simply referred to as carbon, oxygen and phosphate) are invoked. It is assumed that there is always enough carbon dioxide available to support photosynthesis. Oxygen is implicitly exchanged with an infinite atmosphere which maintains the surface reservoir at saturation. Phosphate is supplied to the model by a specified riverine flux into the surface reservoir. Carbon and phosphate (in their Redfield ratios) leave the model as a flux of organic particles to the sediments. A steady-state model requires the phosphate flux to the sediments to equal the riverine phosphate flux. Thus the model is externally forced only by the riverine phosphate flux and the atmospheric oxygen level.

The surface and deep reservoirs interact in three ways. Biological activity in the euphotic zone produces a flux of new carbon that settles as particles into the deep reservoir. The bulk of these particles are oxidized in the deep reservoir but a small portion are not oxidized and may accumulate as sediment. The second interaction between the surface and deep reservoirs is the formation of deep water which removes oxygen and phosphate from the surface reservoir and adds oxygen and phosphate to the deep reservoir. The amount of phosphate supplied to the bottom of the deep reservoir by deep water formation depends on the amount of phosphate available in deep water source regions. This phosphate is frequently referred to as preformed phosphate. We will distinguish two modes of bottom water production and hence two modes of the model—a global mode and a basin mode. In the global mode all the water, phosphate and oxygen removed from the surface reservoir is added to the bottom of the deep reservoir. The basin mode only requires that the amount of water added to the bottom of the deep reservoir must equal the amount of water removed from the surface reservoir. In the basin mode, the deep water source may be external to the basin and can act as either a sink or source of phosphate. A concrete present-day example of a situation for which the basin mode is applicable is the supply of Atlantic phosphate to the deep Pacific by Antarctic bottom water (AABW) due to the participation of North Atlantic deep water in the formation of AABW. The third interaction is the advective and diffusive exchange of oxygen and phosphate at the boundary between the top of the deep reservoir and the surface reservoir. The parameterization of these interactions and the governing equations of the two reservoirs will be detailed in the next three subsections.

3.2. Surface reservoir equations

The surface reservoir encompasses the euphotic zone and may include the deep water source regions. The surface reservoir is modeled as a "black box"; i.e. only inputs and outputs are specified and required to balance. The surface concentrations and the exact nature of the processes and their functional dependence on the surface concentrations are not explicitly modeled. The governing phosphate equation for the surface reservoir (for both global and basin modes) expresses the balance of the phosphate fluxes into and out of the surface reservoir (see the Nomenclature for definitions of all variables and parameters):

$$\left(K\frac{\mathrm{d}P}{\mathrm{d}z} + wP\right)_{z=0} + I = \frac{N}{R} + D. \tag{1}$$

The term in parentheses represents the diffusive and advective fluxes of phosphate across the boundary between the top of the deep reservoir (i.e. at $z = 0$) and the surface reservoir. The term I is the riverine phosphate flux, N/R represents the removal of phosphate from the euphotic zone, as particles, by the biogenic production of new carbon (N) (where R is the Redfield ratio) and D

represents the removal of phosphate from the surface reservoir forced by deep water formation. D is defined as

$$D = wP_D, \tag{2}$$

where P_D is the phosphate concentration of the water removed from the surface reservoir. P_D is determined by the amount of phosphate not removed from the euphotic zone by the production of new carbon. P_D is specified by introducing the parameter ξ, such that

$$D = \xi wP(z = 0). \tag{3}$$

A totally nutrient-limited surface reservoir would correspond to $\xi = 0$. We will show that present-day phosphate profiles require ξ to be in the range 3–6. Defining the new-carbon flux as vC_0 (where v is the settling velocity) and $P(z = 0)$ as P_0, allows the surface reservoir governing equation to be written as

$$K\frac{\mathrm{d}P}{\mathrm{d}z}\bigg|_{z=0} + I = \frac{vC_0}{R} + (\xi - 1)wP_0. \tag{4}$$

3.3. Deep reservoir equations

In the deep reservoir the distributions of carbon, oxygen and phosphate are modeled by

$$v\frac{\mathrm{d}C(z)}{\mathrm{d}z} + \Omega C(z)\Theta(O(z)) = 0, \tag{5}$$

$$K\frac{\mathrm{d}^2O(z)}{\mathrm{d}z^2} + w\frac{\mathrm{d}O(z)}{\mathrm{d}z} - \eta\Omega C(z)\Theta(O(z)) = 0 \tag{6}$$

and

$$K\frac{\mathrm{d}^2P(z)}{\mathrm{d}z^2} + w\frac{\mathrm{d}P(z)}{\mathrm{d}z} + \frac{\Omega}{R}C(z)\Theta(O(z)) = 0. \tag{7}$$

The carbon equation simply states that the divergence of the carbon flux is equal to the carbon consumption. The consumption of carbon must depend on the properties and composition of the particular oxidizable material. The parameter Ω is interpreted as representing an average value of the rate constant for the consumption process. Similarly, the organic particles have a wide spectrum of sizes, shapes and densities. The settling velocity (v) is interpreted as an average value. The consumption rate is assumed to be first order in carbon and independent of oxygen wherever oxygen is present. Where oxygen vanishes, consumption ceases and hence the step function. The oxygen and phosphate equations simply state that the flux divergences (both diffusive and advective) are equal to sink and source terms which are themselves proportional to the carbon consumption rate. The symbols O and P are the oxygen and phosphate concentrations respectively, K is the eddy diffusion coefficient, w the vertical (or abyssal upwelling) velocity and R is the Redfield ratio. The parameter η ($\cong 1.4$, [9]) accounts for the fact that more oxygen is consumed than carbon dioxide produced when the debris of marine plankton is burned. This is because material in addition to carbon is being oxidized.

3.4. Boundary conditions

The appropriate boundary conditions at the top of the deep reservoir are that carbon, oxygen and phosphate concentrations are

$$C(z = 0) = \frac{N}{v} = C_0, \tag{8a}$$

$$O(z = 0) = O_0 \tag{8b}$$

and

$$P(z = 0) = P_0. \tag{8c}$$

The carbon boundary condition (8a) is formulated by expressing the carbon flux into the deep reservoir as a concentration (C_0) times a settling velocity (v) and equating it to the new-carbon flux (N). The oxygen boundary condition results from assuming that the surface reservoir is maintained at saturation by an infinite atmosphere, so the value O_0 is determined by the atmosphere. The value of P_0 is taken from data.

Flux boundary conditions specify the fluxes of oxygen and phosphate at the bottom of the deep reservoir (due to bottom water formation) as

$$\left(K\frac{dO}{dz} + wO\right)\Big|_{z=h} = F_O = wO_D = \zeta wO_0 \tag{9a}$$

and

$$\left(K\frac{dP}{dz} + wP\right)\Big|_{z=h} = F_P = wP_{PF} = \xi' wP_0. \tag{9b}$$

The symbols F_O and F_P represent the fluxes of oxygen and phosphate (preformed phosphate), respectively, into the deep reservoir due to deep water formation. Continuity requires the flow of water out of the surface reservoir to be equal to w. Hence it is reasonable to define effective concentrations of oxygen and phosphate O_D and P_{PF} in the source regions. The parameters ζ and ξ' are introduced so that these concentrations can be expressed in terms of the oxygen (O_0) and phosphate (P_0) concentrations at $z = 0$. In the global mode the phosphate flux out of the surface layer (D) equals the preformed phosphate flux, so $P_D = P_{PF}$, and $\xi' = \xi$. If abyssal vertical phosphate gradients are small (as they are in the present-day ocean) ξ' like the others is very nearly the ratio of the phosphate concentrations at the bottom and top of the deep reservoir. Because our formulation treats the oceans as an open system with respect to oxygen no distinction is made with regards to oxygen between the global and basin modes. The parameter ζ represents the fact that the oxygen concentration in deep water may be different from that in the source region because of temperature effects and the fact that deep water formation sites are not quite maintained at saturation. Thus the fluxes of oxygen and phosphate due to deep water formation are proportional to the concentrations at $z = 0$, the vertical velocity (w) and the parameters ζ and ξ'.

3.5. Scaling

The solutions are the consequence of interplay between physical, chemical and biological processes. Hence, a large number of parameters, which characterize these processes, appear as coefficients in the governing equations. To simplify the discussion of the model we have scaled the solutions, thus reducing the number of parameters. There are two natural length scales: K/w, i.e. diffusivity over vertical velocity or the pycnocline scale height; and v/Ω, i.e. settling velocity over oxygen consumption rate constant, or carbon scale height. We have chosen to scale depth by the carbon scale height, [which for convenience we will refer to by its reciprocal ($\alpha = \Omega/v$)].

The model solutions are completely characterized by the following three dimensionless numbers and the parameters appearing in the boundary conditions. These numbers are

$$w_v = \frac{w}{K\dfrac{\Omega}{v}} = \frac{w}{K\alpha} \quad \text{(ventilation number)}, \tag{10}$$

$$v_w = \frac{\eta v C_0}{K\dfrac{\Omega}{v}O_0} = \frac{\eta v C_0}{K\alpha O_0} \quad \text{(Wyrtki number)} \tag{11}$$

and

$$v_n = \frac{vC_0}{RK\frac{\Omega}{v}P_0} = \frac{vC_0}{RK\alpha P_0} \quad \text{(nutrient number)}. \tag{12}$$

The ventilation number is the ratio of the two scale heights. We have expressed this ratio with w appearing in the numerator and chose the symbol w_v to emphasize that it can also be interpreted as a scaled vertical velocity. Note the vertical velocity does not appear in either of the other two dimensionless numbers. The Wyrtki number [equation (11)] is the ratio of two fluxes [10]. The numerator is proportional to the new-carbon flux out of the surface reservoir and represents the potency of the oxygen sink in the deep reservoir. The denominator has the form of a diffusive oxygen flux, i.e. an eddy diffusivity times an oxygen gradient. Thus the Wyrtki number expresses the balance between the oxygen sink and the downward flux of oxygen from the surface reservoir, in the absence of vertical advection and can be interpreted as a scaled new-carbon flux. Similarly, the nutrient number [equation (12)] expresses the balance between the phosphate source (nutrient regeneration) and the phosphate flux to the surface reservoir from below, in the absence of advection.

The flux of new carbon from the surface reservoirs appears in the numerator of both the Wyrtki and nutrient numbers, so

$$v_n = \frac{O_0}{\eta R P_0} v_w. \tag{13}$$

Choosing present-day values of η, R, O_0 and P_0 in equation (13) allows us to eliminate the nutrient number and thus discuss the profiles in terms of the two dimensionless numbers (i.e. w_v and v_w). However, it should be cautioned that the relationship expressed in equation (13) may have varied through geologic time. In Subsection 5.2 the model is calibrated with present-day data. It is shown that all the dimensionless parameters are of order 1 so that no terms can be dropped from the solutions.

4. MODEL SOLUTIONS

4.1. Oxic case

For the oxic case, equation (5) describes the carbon distribution. Its solution is

$$C(z) = C_0 e^{-\alpha z} \qquad 0 \leqslant z \leqslant h. \tag{14}$$

Sediment trap data [11] are consistent with an exponential depth dependence. The length scale for the decrease of carbon consumption is $\frac{1}{\alpha} = v/\Omega$.

The oxygen and phosphate solutions are

$$\frac{O(z)}{O_0} = A_1 + A_2 \exp(-w_v \alpha z) + A_0 \exp(-\alpha z) \quad 0 \leqslant z \leqslant h \tag{15}$$

and

$$\frac{P(z)}{P_0} = B_1 + B_2 \exp(-w_v \alpha z) - B_0 \exp(-\alpha z) \quad 0 \leqslant z \leqslant h \tag{16}$$

Expressions for the coefficients A_i and B_i are given in the Appendix. The coefficients are completely specified by the dimensionless numbers and the depth of the deep reservoir (h). The oxygen profiles depend on the Wyrtki number and the ventilation number. The phosphate profiles depend on the

nutrient number and the ventilation number. In our analysis we use equation (13) to relate the nutrient number to the Wyrtki number. There is a constraint imposed by the model on the flux of new carbon out of the surface reservoir and hence on the Wyrtki number. This constraint is derived by substituting equation (16) into equation (4), yielding

$$vC_0 = R\,e^{\alpha h}[I + (\xi' - \xi)wP_0]. \tag{17}$$

For the global mode where the flux of dissolved phosphate out of the surface reservoir equals the flux of preformed phosphate (i.e. $\xi' = \xi$) the globally averaged new-carbon flux is constrained by the riverine phosphate flux (I) and is independent of: the rate of deep water production (w), extent of nutrient limitation (ξ) or details of mixing (K). Equation (17) also expresses a necessary condition for a steady-state global ocean: the particle flux of phosphate out of the bottom ($vC_0\,e^{-\alpha h}/R$) must exactly balance the riverine phosphate flux.

4.2. Anoxic case

When anoxia occurs in the deep reservoir, three layers can be distinguished: an anoxic layer sandwiched between shallow and deep oxic layers. Figure 2 is a schematic sketch of these layers. The depths of the upper and lower boundaries of the anoxic layer (h_1 and h_2) are determined from the oxygen equation and appropriate matching conditions. The determination of these depths is discussed below. When anoxic conditions exist in the depth range $h_1 \leqslant z \leqslant h_2$ the carbon profile becomes

$$C(z) = \begin{cases} C_0 \exp(-\alpha z) & 0 \leqslant z \leqslant h_1 \quad (18a) \\ C_0 \exp(-\alpha h_1) & h_1 \leqslant z \leqslant h_2 \quad (18b) \\ C_0 \exp(-\alpha h_1)\exp[-\alpha(z - h_2)] & h_2 \leqslant z \leqslant h. \quad (18c) \end{cases}$$

In the oxic layers ($0 \leqslant z \leqslant h_1$) and ($h_2 \leqslant z \leqslant h$) the distribution shows an exponential decrease with depth.

Oxygen and phosphate profiles in the deep reservoir are solutions to equations (6) and (7). For the anoxic case, equations (18a–c) provide the carbon concentration appearing in the source and sink terms. The oxygen and phosphate solutions are

$$\frac{O(z)}{O_0} = \begin{cases} A + A_2 \exp(-w_v \alpha z) + A_0 \exp(-\alpha z) & 0 \leqslant z \leqslant h_1 \quad (19a) \\ 0 & h_1 \leqslant z \leqslant h_2 \quad (19b) \\ A_3 + A_4 \exp[-w_v \alpha (z - h_2)] + A_0 \exp(-\alpha h_1)\exp[-\alpha(z - h_2)] & h_2 \leqslant z \leqslant h \quad (19c) \end{cases}$$

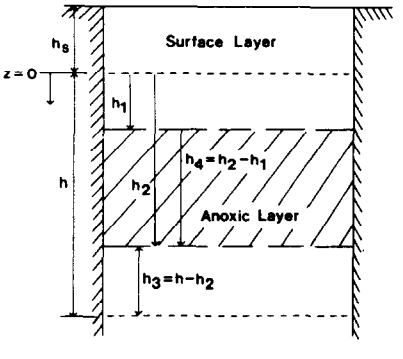

Fig. 2. Sketch of the model domain when anoxia occurs with the various layer thicknesses defined.

and

$$\frac{P(z)}{P_0} = \begin{cases} B_1 + B_2 \exp(-w_v \alpha z) + B_0 \exp(-\alpha z) & 0 \leqslant z \leqslant h_1 \quad (20a) \\ B_3 + B_4 \exp[-w_v \alpha (z - h_1)] & h_1 \leqslant z \leqslant h \quad (20b) \\ B_5 + B_6 \exp[-w_v \alpha (z - h_2)] - B_0 \exp(-\alpha h_1) \exp[-\alpha (z - h_2)] & h_2 \leqslant z \leqslant h. \quad (20c) \end{cases}$$

Expressions for the coefficients A_i and B_i can be found in the Appendix. The coefficients depend on the Wyrtki number, nutrient number and depth of the deep reservoir.

The depths to the top and bottom of the anoxic layer, h_1 and h_2 respectively, and the coefficients (A_i) for the oxygen profiles are determined by applying appropriate matching conditions to the oxygen solution. Clearly, necessary and sufficient conditions for the occurrence of anoxia are that $0 \leqslant h_1 \leqslant h_2 \leqslant h$. The depth to the top of the anoxic layer is determined by boundary condition (8a) at $z = 0$ and the matching conditions at $z = h_1$:

$$O(z = h_1) = 0 \quad (21a)$$

and

$$\left.\frac{dO}{dz}\right|_{z=h_1} = 0. \quad (21b)$$

These conditions are a statement that the vertical flux of oxygen at the depth $z = h_1$ vanishes. Applying them to equation (19a) yields a transcendental equation for αh_1:

$$1 - \frac{1}{v_w}(1 - w_v) - \exp(-\alpha h_1)\left\{1 + \frac{1}{w_v}[\exp(w_v \alpha h_1) - 1]\right\} = 0 \quad (22)$$

The scaled depth, αh_1, is a measure of how effectively the deep reservoir is ventilated by turbulent mixing from above.

Figure 3 is a plot of families of αh_1 vs ventilation number determined from equations (21a, b) for various Wyrtki numbers. For small values of the ventilation number (i.e. $w_v \ll 1$) and values of the Wyrtki number < 1.0, sufficient oxygen is supplied downward from the surface reservoir by the diffusive process to maintain an oxygenated deep reservoir regardless of the magnitude of the oxygen flux at the bottom. With increasing vertical circulation the upward advective flux dominates over this downward diffusive flux leading to a decrease in the net flux of oxygen from the surface reservoir to the deep reservoir. For Wyrtki numbers > 1.0 the balance between oxygen consumption and oxygen transport from the surface reservoir may lead to anoxic conditions.

The depth of the bottom of the anoxic layer (h_2) is controlled by the rate at which oxygen is supplied to the bottom of the deep reservoir by deep water production. The appropriate matching conditions at the bottom of the anoxic layer are:

$$O(z = h_2) = 0 \quad (23a)$$

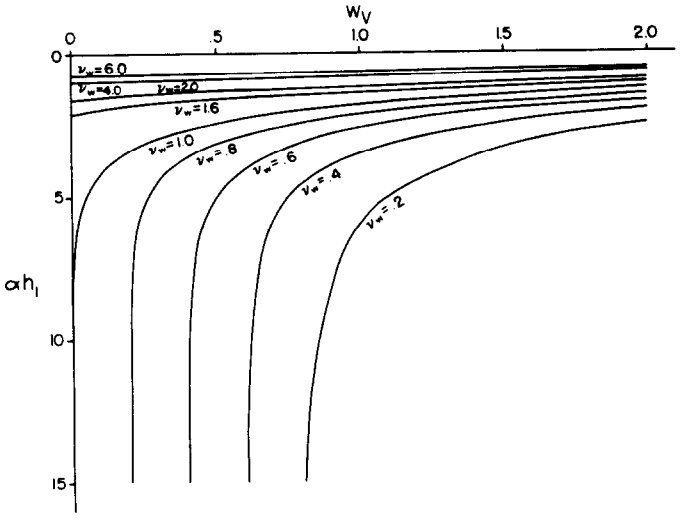

Fig. 3. Plot of αh_1, the scaled depth to the top of anoxic layer (see Fig. 2) as a function of the ventilation number (w_v), defined in equation (17). Each curve corresponds to a fixed Wrytki number [ν_w, defined in equation (8)].

and

$$\left.\frac{dO}{dz}\right|_{z=h_2} = 0. \tag{23b}$$

These conditions are a statement that there is no flux of oxygen into the anoxic layer from below. The above matching conditions, the flux boundary conditions at the bottom of the deep layer ($z = h$) together with equation (19c) leads to the following equation in αh_3 and αh_1:

$$\alpha h_3 = -\ln\left[1 - \frac{w_v \zeta}{\nu_w \exp(-\alpha h_1)}\right]. \tag{24}$$

Figure 4 is a plot of families of the quantity $\alpha(h_1 + h_3)$, i.e. the total thickness of the oxygenated water column, vs the ventilation number for a suite of Wyrtki numbers. In Fig. 4 small values of

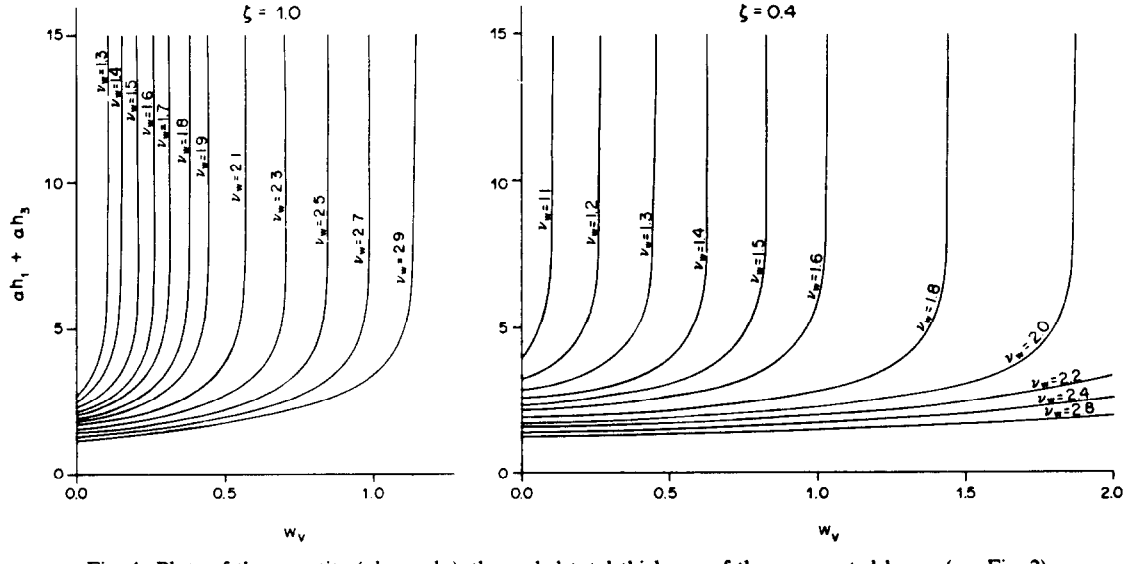

Fig. 4. Plots of the quantity ($\alpha h_1 + \alpha h_3$), the scaled total thickness of the oxygenated layers (see Fig. 2) as a function of the ventilation number (w_v).

$\alpha(h_1 + h_3)$ correspond to thick anoxic layers. Clearly, if $\alpha(h_1 + h_3)$ is greater than the depth of the basin under consideration an anoxic layer cannot exist. For any given set of the parameters w_v, h and ζ there is a critical Wyrtki number that denotes the onset of anoxia. For any given Wyrtki number, the quantity $\alpha(h_1 + h_3)$ undergoes an abrupt transition from a slowly varying to a rapidly varying function of the ventilation number. This is because the rate of oxygen supplied at the bottom of the deep reservoir is a function of w_v. For small w_v, carbon production in the surface layer, reflected in the Wyrtki number, determines $\alpha(h_1 + h_3)$. With increasing w_v the oxygen supplied at the bottom prevents the deep reservoir from developing anoxia.

The depths h_1 and h_2 determined from the oxygen solution (19a–c) along with appropriate matching conditions are used to determine the coefficients B_i $(i = 0, \ldots 6)$ appearing in the phosphate solution (20a–c). The appropriate matching conditions are that the phosphate profiles and derivatives with respect to depth are continuous across the oxic–anoxic interface at $z = h_1$ and h_2. This yields a set of linear equations for the coefficients B_i (see the Appendix). Substitution of equation (20a) into equation (4) leads to a constraint on the carbon flux (vC_0) from the surface reservoir analogous to equation (17):

$$vC_0 = R \exp[\alpha(h_1 + h_3)][I + (\xi' - \xi)wP_0]. \tag{25}$$

Again one can distinguish between the global mode ($\xi' = \xi$) and the basin mode ($\xi' \neq \xi$). For a steady state to exist the riverine phosphate flux into the surface reservoir must balance the phosphate flux in particles out of the model. However, in contrast with the oxic case, the net carbon flux is no longer independent of the rate of vertical circulation. The argument of the exponent $\alpha(h_1 + h_3)$, is functionally dependent on the ventilation number. Therefore, the balance dictated by equation (25) will be different for different ventilation numbers.

5. MODEL PROFILES

This section examines the functional dependence of carbon, oxygen and phosphate profiles on the parameters appearing in the model. The first subsection will be a brief summary of these parameters, that will be useful for understanding the ensuing discussion, particularly for readers who have declined to read the detailed discussion of the model and its solutions in Sections 3 and 4. In the next subsection the model is calibrated with present-day data. Finally, hypotheses for the occurrence of large-scale anoxia are explored with a set of model-parameter sensitivity experiments. The hypotheses which the experiments address are: (1) fertility, (2) stagnation or reduced thermohaline circulation and (3) the WSBW hypothesis based on oxygen solubility.

5.1. Summary of model parameters

In Section 3 the many parameters that appear in the model were collected into a few dimensionless numbers. The model results are presented in terms of these numbers. Their formal definitions can be found in Section 3 or the Nomenclature. The purpose of this subsection is to show that these numbers can be interpreted in terms of familiar quantities and to provide a readily accessible guide to interpreting the figures and discussion.

The profiles can be described in terms of the Wyrtki number, the ventilation number and the dimensionless boundary condition parameters. The Wyrtki number can be interpreted as the scaled new-carbon flux from the euphotic zone and hence as an index of fertility. Below it is shown that the present-day global Wyrtki number is very close to 1 and that the global calibration implies a new-carbon flux of 0.65 mol C/yr m^2. The other dimensionless number is the ventilation parameter which has the interpretation of a scaled vertical velocity. It is shown below that the present-day global ventilation number is very close to 1 and that the global calibration implies a vertical velocity of 4×10^{-3} km/yr which corresponds to a bottom water formation rate of about 40 sverdrups.

The dimensionless boundary condition parameters do not have quite as satisfactory intuitive interpretations as do the Wyrtki and ventilation numbers. They should be thought of as parameters determined by the calibration. They represent the variety of processes that determine that abyssal

properties from the properties in the deep water source regions. The parameter ζ is determined from the oxygen calibration. The parameters ξ and ξ' are determined by the phosphate calibration in the global and basin mode, respectively (see the next paragraph for a brief discussion of the global and basin modes).

The model has two modes, a global mode and a basin mode. In the basin mode the deep water formation source region can be external to the surface reservoir and may act as either a source or sink or phosphate. In the global mode the deep water source region is in the surface reservoir and the only external source of phosphate is the riverine flux. In the global mode, up to the onset of anoxia, the Wyrtki number can be written as

$$v_w = \frac{\eta R I e^{\alpha h}}{\alpha K O_0} \tag{26}$$

and the ventilation number as

$$w_v = \frac{w}{\alpha K}. \tag{27}$$

Since these two dimensionless numbers (plus the boundary condition parameters) completely describe the oxygen profiles, one can interpret changes in any parameter that appears in only one of these numbers (only α and K appear in both) as a change in that number. For example, changes in the Redfield ratio (R) can be represented by changes in the Wyrtki number. Thus an experiment to ascertain the attainment of anoxia over a range of Wyrtki numbers can be interpreted as an experiment over a range of Redfield ratios or atmospheric oxygen levels (O_0) etc. Note that if η, R or O_0 is changed, phosphate profiles must be recalculated [see equation (13)].

5.2. Model calibration

The most appropriate data sets for calibration are those from Levitus [12] and the GEOSECS expedition. Levitus [12] calculated both global and basin-wide mean oxygen profiles from NODC data files consisting of approx. 0.5 million stations. Unfortunately, the Levitus data does not include phosphate. Comparison is first made between the Levitus and GEOSECS oxygen data to justify the use of the sparser GEOSECS data to represent global and basin wide mean oxygen and phosphate profiles.

Figure 5a includes the global Levitus oxygen profile (×) and a simple basin-area weighted mean oxygen profile of the GEOSECS data (○). The close agreement between the two profiles suggests that the same simple weighting of the GEOSECS phosphate data may be interpreted as a global mean phosphate profile (Fig. 5b). The curves in Figs 5a, b are model results that represent reasonable fits to the global oxygen and phosphate data. The paucity of sediment trap data precludes the construction of a global mean carbon profile. However, model prediction of organic-carbon fluxes will be discussed below. The values of the model parameters from the global calibration are summarized in Table 1.

The basin mode of the model is calibrated by consideration of Atlantic and Pacific data. Figures 6a and 7a include both Levitus and GEOSECS oxygen data for the Atlantic and Pacific, respectively, and Figs 6b and 7b GEOSECS phosphate data. Again the curves are fits of model profiles to the data. The carbon scale height from the global calibration was used for the basin mode calibrations. The assumption being that the oxidation rate by micro-organisms and settling velocity of organic particles is the same in both oceans. The differences in profiles are then a consequence of differences in parameters describing: the flux of new carbon, rate of abyssal upwelling, ventilation and preformed nutrients. Comparison of the Atlantic and Pacific profiles show the distributions of oxygen and phosphate in the two oceans to be substantially different. These differences will be discussed below in the context of differences in model parameters. The agreement between the model profiles and data, shape and position of extrema, suggests that the model is reasonably capable of describing present-day global and basin-wide oxygen and phosphate systems.

This reasonable agreement between the model profiles and global data allows an estimation of

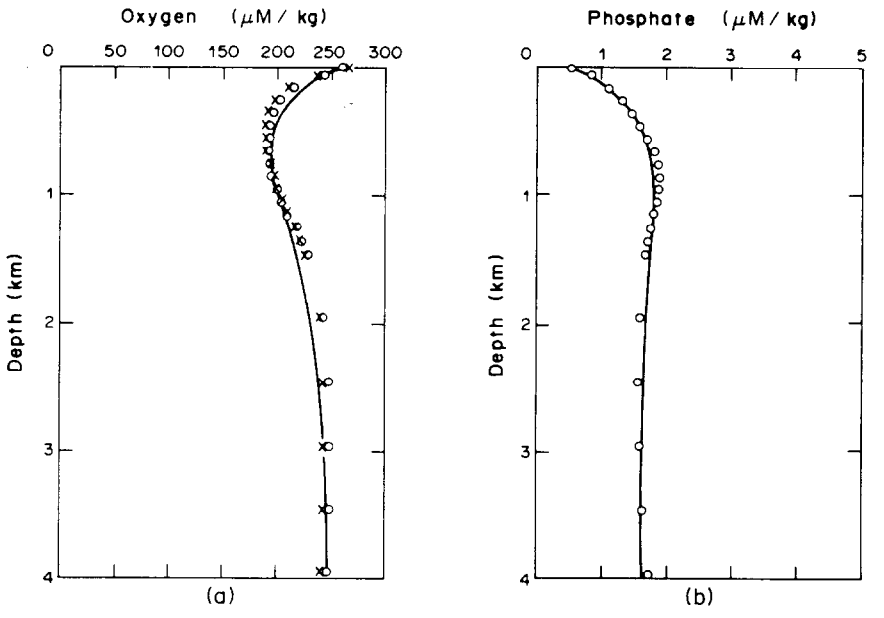

Fig. 5. Calibration of global mode: (a) global Levitus oxygen profile (×), basin-area weighted mean oxygen profiles of Atlantic and Pacific GEOSECS data (○) and model fit to global oxygen data (——); (b) basin-area weighted mean phosphate profiles of Atlantic and Pacific data (○) and model fit to the global GEOSECS phosphate data (——).

Table 1. Model calibration

		Global	Atlantic	Pacific
α (km^{-1})	Carbon consumption scale height	1.2	1.2	1.2
w_*	Ventilation number	1.0	1.95	0.9
ζ	Boundary condition parameter	0.83	0.95	0.74
ξ	Boundary condition parameter	4.4	3.0	5.4
ν_*	Wyrtki number	0.92	0.86	0.95
O_0 (μM/kg)	Oxygen concentration at $z = 0$	250	265	245
P_0 (μM/kg)	Phosphate concentration at $z = 0$	0.5	0.5	0.5
$\frac{{}^*K}{w}$ (m)	Pycnocline scale height	830	430	930
*T (yr)	Residence time	1000	510	1110

*Values calculated assuming a global residence time of 10^3 yr.

the global new-carbon flux and the riverine flux of phosphate to the world ocean (see the following section for values and discussion). The mean new-carbon flux for the present-day Atlantic and Pacific are also calculated. However, the riverine flux of phosphate to the Atlantic and Pacific cannot be estimated because of uncertainty in the estimate of the net exchange of phosphate between these two basins.

Having calibrated the model with present-day oxygen and phosphate on a global and basin-wide scale we feel justified in performing sensitivity experiments to provide insight into the possible causes of large-scale oceanic anoxia. The sensitivity experiments are designed to help distinguish between hypotheses for the existence of a steady-state anoxic ocean. The sensitivity experiments are conducted by varying a single model parameter at a time, all other parameters retaining their calibration values.

5.3. *Fertility experiment*

Figures 8a–c are families of global mode oxygen, phosphate and carbon profiles, for a suite of Wyrtki numbers. Recall that the Wyrtki number has the interpretation of a scaled new-carbon flux, with larger Wrytki numbers corresponding to higher fertility. Each model profile in Figs 8a–c corresponds to a value of Wyrtki number between 0.6 (extreme right) and 4.0 (extreme left) in increments of 0.2. All the other parameters are the same as the global calibration (Figs 5a, b). The global GEOSECS data and global calibration (heavy curve) are also shown for reference.

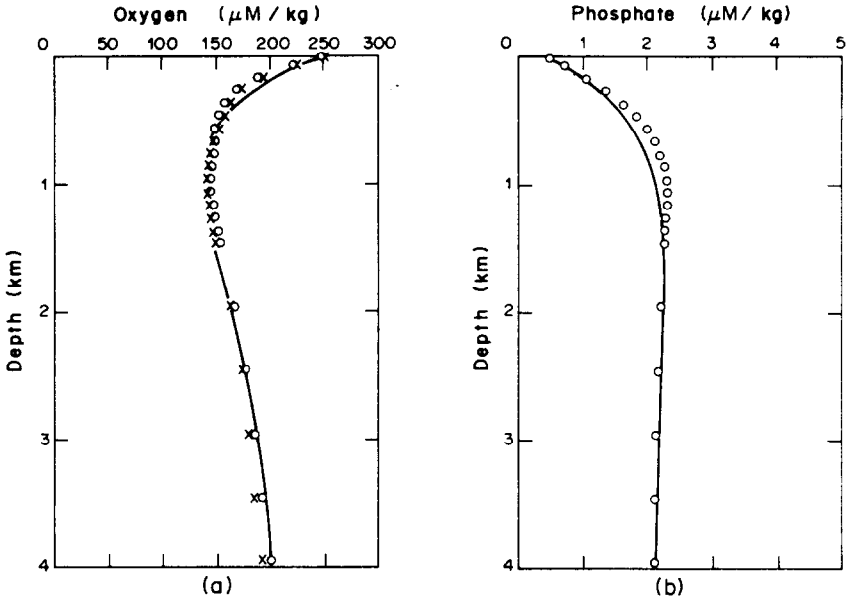

Fig. 6. Calibration of basin mode: (a) Atlantic Levitus oxygen profile (×), Atlantic GEOSECS oxygen data (○) and model fit to Atlantic data (——); (b) Atlantic GEOSECS phosphate data (○) and corresponding model fit to Atlantic GEOSECS data (——).

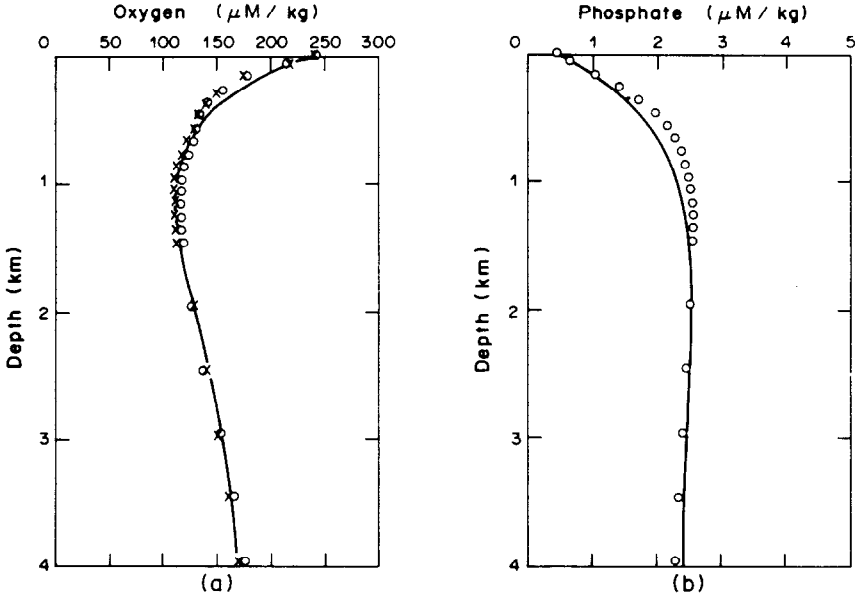

Fig. 7. Calibration of basin mode: (a) Pacific Levitus oxygen profile (×), Pacific GEOSECS phosphate data (○) and model fit to Pacific (——) data; (b) Pacific GEOSECS phosphate data (○) and corresponding model fit to Pacific GEOSECS data (——).

The oxygen profiles corresponding to Wrytki numbers <2.6 describe totally oxic conditions. For oxic profiles the oxygen minimum occurs at a depth of approx. 1.0 km. The oxygen value at the minimum decreases with increasing Wyrtki number. This is a consequence of oxygen consumption increasing with increasing production of new carbon. Anoxic conditions develop when the Wyrtki number exceeds a critical threshold value. In Fig. 8a the critical Wyrtki number, is a little larger than 2.6. A value of $v_w = 2.6$ corresponds to oxic conditions while for $v_w = 2.8$ a thick anoxic layer has developed. This transition from oxic to anoxic conditions is a very sensitive function of v_w. With each incremental increase of 0.2 in Wyrtki number above the critical value,

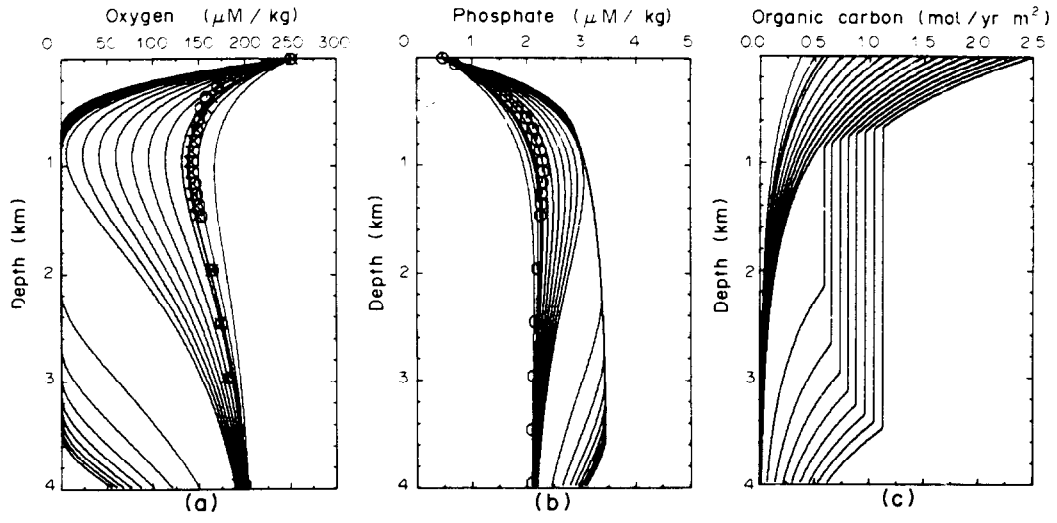

Fig. 8. Global fertility experiment. Families of global mode oxygen (a), phosphate (b) and carbon flux (c) profiles, for a suite of Wrytki numbers. Each model profile corresponds to a fixed Wrytki number in the range 0.6–4.0 in increments of 0.2. All profiles are for a ventilation number $w_v = 1.0$ and the bottom flux boundary conditions on oxygen and phosphate correspond to $\zeta = 0.83$ and $\xi = 4.4$.

the increase in thickness of the anoxic layer is substantial even though we are neglecting nitrate and sulphate reduction. At the onset of anoxia, the oxygen supplied by deep water formation is entirely consumed below the anoxic layer. This could have been surmised by inspection of Fig. 4 for a given fixed w_v. Note that the oxygen value at 4 km is not a fixed value but adjusts to satisfy the constant flux boundary condition.

The corresponding families of global mode phosphate and carbon profiles are shown in Figs 8b, c. The character of the profiles undergoes a dramatic change at the onset of anoxia ($v_w > 2.6$). With the onset of anoxia the flux of carbon reaching a depth of 4 km has drastically increased. The model overpredicts this flux because of the neglect of nitrate and sulphate reduction.

For the global mode the Wyrtki number, and hence the fertility, are directly proportional to the river input of phosphate. Comparing the global calibration Wyrtki number ($v_w = 0.92$) with the critical value ($v_w \approx 2.6$) suggests that in order for the present-day global ocean to achieve steady-state anoxia, fertility and ultimately the river phosphate load, would have to be almost three times present-day values.

5.4. Reduced thermohaline circulation experiment

Stagnation and/or increased stratification are frequently cited as causes of oceanic anoxia. Some confusion exists in the paleoceanographic literature concerning the relation between stratification and intensity of thermohaline circulation. A steep pycnocline has sometimes been interpreted as a consequence of stagnation. Thermohaline circulation together with interior mixing processes determines the pycnocline scale. The more vigorous the thermohaline circulation the steeper the gradient adjacent the mixed layer. The sharp density contrast between waters of the mixed layer and adjacent depths is actually maintained by vigorous vertical circulation.

To test the hypothesis that anoxia is a consequence of stagnation or a reduced thermohaline circulation rate, global mode sensitivity experiments were performed on the ventilation number (w_v). Recall the ventilation number is proportional to the vertical advective velocity. Its value characterizes the rate of bottom water formation or rate of thermohaline circulation. The results of two thermohaline circulation rate experiments will be considered: a "sluggish ocean" with w_v equal one half the global calibration value, and a "stagnant ocean" with $w_v = 0$.

The results of the "sluggish global ocean" experiment are shown in Figs 9a, b. These figures are families of oxygen and phosphate profiles, for the same suite of Wyrtki numbers and parameters values as the fertility experiment except the ventilation parameter has been halved. The thick curve again has the same Wyrtki number as the global calibration curve and the global GEOSECS data is shown for reference. Comparison between Figs 9a, b and Figs 7a, b demonstrates the sensitivity

of the model oxygen and phosphate profiles to the thermohaline circulation rate. Note the difference in profiles shapes and the depths of the oxygen minimum and phosphate maximum. The value of the critical Wyrtki number is $(v_w)_{crit} \approx 1.8$ for the "sluggish global ocean", compared with $(v_w)_{crit} \approx 2.6$ for the present-day global ocean.

An even more dramatic circulation sensitivity experiment results from letting $w_v = 0$, i.e. a "stagnant ocean". Figures 10a, b illustrates the model results for this rather unrealistic situation. The oxygen and phosphate profiles no longer exhibit their characteristic pronounced mid-depth extrema. The critical Wyrtki number lies in the range 1–1.2. The profile corresponding to the global calibration Wyrtki number represented by the thick curve, describes oxic conditions existing over the entire depth range. Enough oxygen is mixed down from the surface layer to prevent anoxia with global new carbon production rate and diffusivity held at the present-day values.

5.5. *WSBW experiment*

The results of the experiment testing the WSBW hypothesis, of reduced ventilation resulting from reduced oxygen solubility, are shown in Figs 11a, b. The relevant parameter for the "WSBW experiments" is ζ, which appears in the oxygen boundary condition at the bottom of the deep reservoir [equation (9)]. Figures 11a, b are families of oxygen and phosphate profiles for the same suite of Wyrtki numbers and parameters as the fertility experiment except that ζ now equals one half the global calibration value. Again the heavy curve is for the same Wyrtki number as the global calibration. The critical Wyrtki number falls to between 1.6 and 1.8. Thus anoxic conditions would not exist in the global ocean if the oxygen flux to the deep ocean were reduced by one half while maintaining the present-day rate of thermohaline circulation and fertility. The model phosphate profiles (Fig. 11b) for Wyrtki numbers < 1.6 are identical to the corresponding phosphate profiles in Figs 7a, b. The phosphate profiles do not respond to the reduced oxygen flux until the onset of anoxia. This contrasts with the "sluggish global ocean" experiment where both the oxygen and phosphate profiles differed from "present-day" prior to the onset of anoxia. The WSBW ocean has a lower fertility threshold, $(v_w)_{crit} \approx 1.6$, than the present-day ocean $(v_w)_{crit} \approx 2.6$.

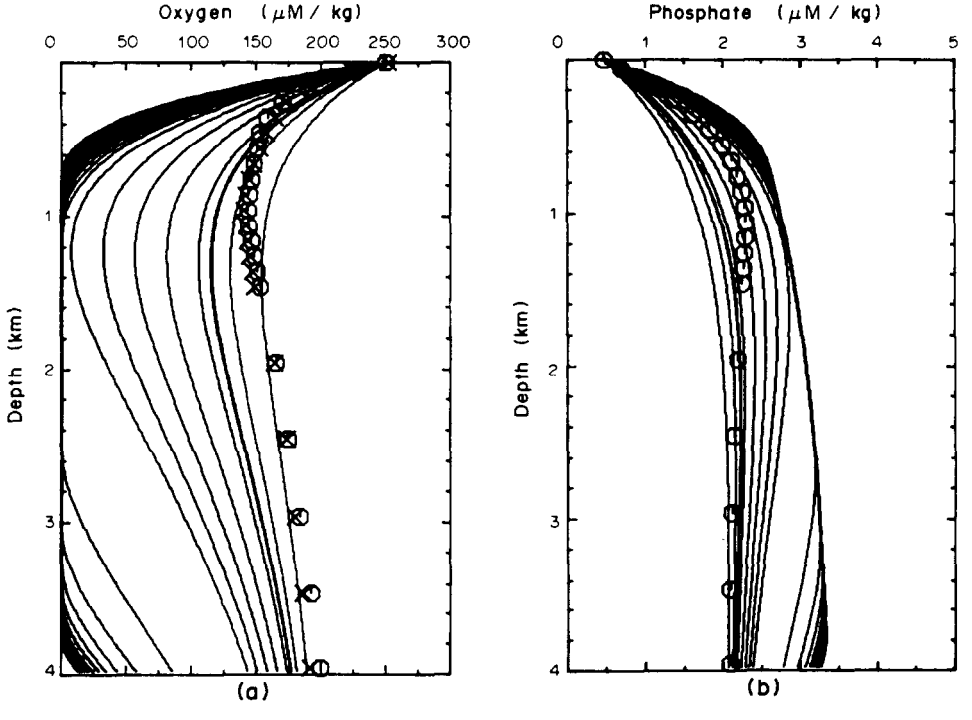

Fig. 9. Sluggish global ocean experiment. Families of global mode oxygen (a) and phosphate (b) model profiles, for a suite of Wrytki numbers. Each model profile corresponds to a fixed Wrytki number in the range 0.6–4.0 in increments of 0.2. All profiles correspond to the reduced ventilation number, i.e. $w_v = 0.5$. The bottom flux boundary conditions on oxygen and phosphate correspond to $\zeta = 0.83$ and $\xi = 4.4$.

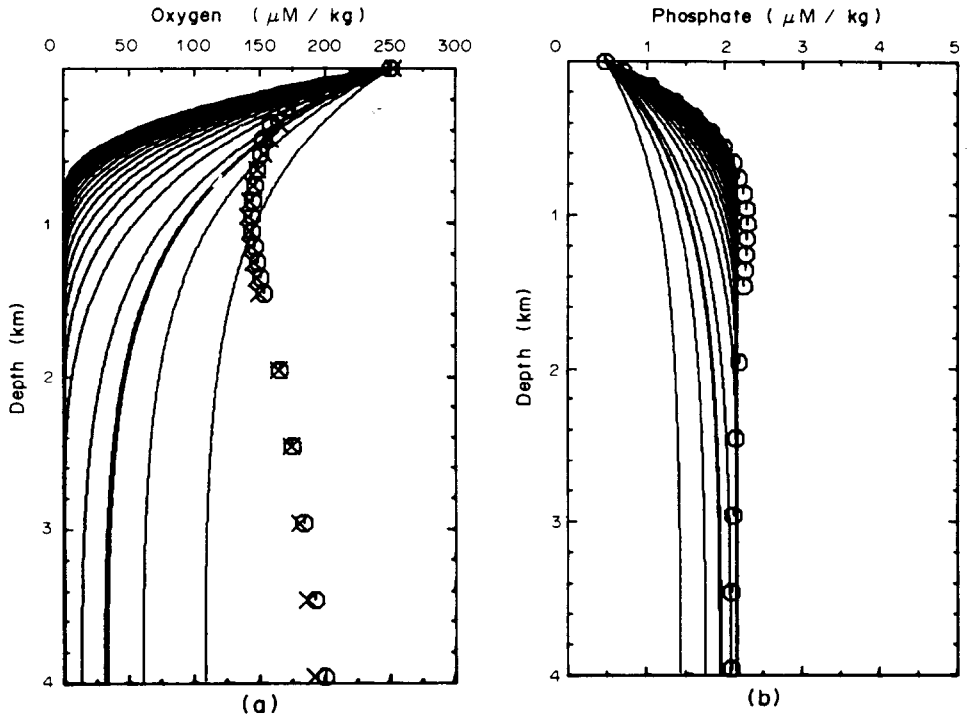

Fig. 10. Totally stagnant ocean experiment. Families of global mode oxygen (a) and phosphate (b) model profiles, for a suite of Wyrtki numbers. Each model profile corresponds to a fixed Wyrtki number in the range 0.6–4.0 in increments of 0.2. All profiles correspond to a "stagnant" ventilation number, i.e. $w_v = 0$. The bottom flux boundary conditions on oxygen and phosphate correspond to $\zeta = 0.83$ and $\xi = 4.4$.

5.6. *Conclusions from the sensitivity experiments*

It is clear that in order to produce steady-state global anoxia our model requires a larger Wyrtki number (greater fertility) than the present-day value. Although reduced circulation and ventilation, reduced the critical Wyrtki number (i.e. require a smaller increase in fertility to produce global anoxia) it is still necessary to increase fertility and hence in a global mode model to increase the riverine phosphate flux. This suggests that the global oceans are rather reluctant to exist in an anoxic steady state. In the Discussion we will further suggest that global anoxia may be a transient phenomena and suggest that the geologic record bears this out.

The Wyrtki numbers appropriate to the present-day Atlantic (0.85) and Pacific (0.95) are close to the global number (0.92)—all being < 1. Repeating the same set of sensitivity experiments for the Atlantic and Pacific basin mode model always yields a critical Wyrtki number > 1. Just as for the global mode, it can be concluded that no single hypothesis would produce basin-scale anoxic conditions in today's Atlantic or Pacific.

6. DISCUSSION

6.1. *Oxic case*

The goal of this study was to formulate the simplest steady-state model which would: (1) describe global and basin-wide mean oxygen, phosphate and carbon profiles, (2) produce global and/or basin-wide anoxia and (3) evaluate proposed hypotheses for the maintenance of steady-state anoxia. The model profiles in Figs 5a, b are in reasonably good agreement with global mean oxygen and phosphate profiles over a substantial portion of the water column. The model profiles place the oxygen and phosphate extrema at the observed depth of approx. 1 km. The largest discrepancies between the model profiles and the data are near the top of the water column. The model oxygen profile represents the balance between transport and consumption of oxygen by a carbon sink which is exponentially distributed. The shape of the phosphate profile represents the necessary

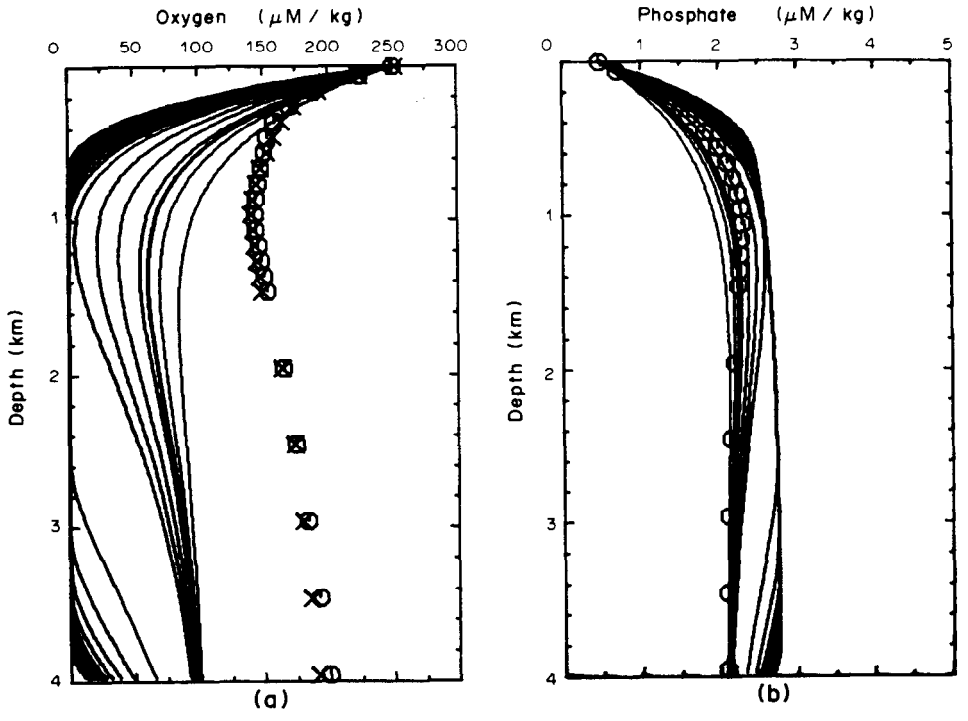

Fig. 11. WSBW experiment. Families of global mode oxygen (a) and phosphate (b) model profiles, for a suite of Wyrtki numbers. Each model profile corresponds to a Wyrtki number in the range 0.6–4.0 in increments of 0.2. All profiles are for a ventilation number $w_v = 1.0$. The bottom flux boundary condition on oxygen has been reduced by half, i.e. $\zeta = 4.2$, and the phosphate parameter remains unchanged at $\xi = 4.4$.

adjustment by the oceans to insure the phosphate flux out of the bottom exactly balances the riverine input.

Using the defining equation for the Wyrtki number [equation (11)] and parameter values from Table 1 the global mean flux of new carbon from the euphotic zone is $N = vC_0 \cong 0.65$ mol C/yr m^2. This new-carbon flux falls at the high end of estimates of new-carbon production based on "classical" ^{14}C techniques [13]. However, Jenkins and Goldman [13], using ^{3}He–^{3}H dating, calculate $N = 4$–5 mol C/yr m^2 for the Sargasso Sea. The value of global new-carbon flux calculated from consideration of the global mean oxygen profile is the result of integrating over large space and time scales and thus represents the average results of processes which are both heterogeneous and transient. Thus comparison with local estimates of the new-carbon flux may not be entirely relevant.

Our results are most properly interpreted as a lower limit of estimates of new-carbon production. However, our model could easily be modified by the addition of a second, more labile type of carbon characterized by a larger oxidation rate or smaller carbon scale height. This carbon would be oxidized and nutrients released high in the water column. This modification would improve the model fits to both the oxygen and phosphate profiles high in the water column where the greatest discrepancy with data exists. Preliminary calculations suggest that a better model fit to the data would be achieved by including a second type of rapidly oxidizing carbon which would increase the new-carbon flux by a factor of 3–4. Thus our best estimate of new-carbon production would be larger than that obtained by ^{14}C but smaller than Jenkins and Goldman's [13] value by a factor of 2–3. However, invoking this additional labile carbon with additional parameters is not in the spirit of the simplest model capable of producing anoxia with the fewest number of parameters.

The formulation of the model explicitly conserves phosphate globally. This allows estimation of the global riverine phosphate flux from the global calibration. A necessary condition for the global ocean t be in a steady state is that the input of phosphate from rivers must be exactly balanced

by the output of phosphate incorporated in particles leaving the deep reservoir. From equation (17),

$$I = \frac{vC_0}{R} e^{-ah} = 0.43 \times 10^{-4} \text{ mol P/yr m}^2.$$

This value is in remarkable agreement with the value of 0.4×10^{-4} mol P/yr m^2 for the burial flux of organic phosphate, obtained by measuring the accumulation rate and content of various types of marine sediments [14]. However, our calculation did not treat the following phosphate removal mechanisms: (1) removal with phosphorites, (2) burial with phosphatic fish debris, (3) burial with biogenic calcium carbonates and (4) inorganic removal. Thus our estimate of riverine phosphate flux based solely on the burial flux of organic phosphate represents a lower limit. However this value is in reasonable agreement with estimates of preagricultural phosphate river flux, $1 \pm 0.5 \times 10^{-4}$ mol P/yr m^2 [14].

Comparison of the Atlantic and Pacific oxygen data (Figs 6a and 7a) suggests quite different oceanographic regimes. Quantitative comparison of these differences in fertility, circulation, ventilation and supply of preformed nutrients between the Atlantic and the Pacific can be made by comparing the model parameters for the calibrations in Table 1. Compared to the Atlantic, the Pacific (1) has a slightly larger mean production of new carbon, (2) has a more sluggish abyssal upwelling, (3) is less well ventilated and (4) the deep Pacific receives a larger flux of preformed phosphate. The differences between the Atlantic and Pacific profiles are primarily a consequence of the large difference in the thermohaline circulation rates. The model results suggest that the vertical velocity in the Atlantic is approximately twice that of the Pacific. This result is consistent with the results of Stuiver *et al.* [15]. Using the ^{14}C distribution in abyssal waters they calculate the replacement time for deep waters in the Pacific is approximately twice that of the Atlantic.

Another model prediction which follows as a consequence of globally conserving phosphate is that

$$(v_w)_{Atl} A_{Atl} + (v_w)_{Pac} A_{Pac} = (v_w)_{global}(A_{Atl} + A_{Pac}).$$

This simple "lever" rule weights the Wyrtki number for each basin by the area (A_i) of the basin. The present-day Atlantic has almost twice the area of the Pacific, so that, using the appropriate Wyrtki numbers,

$$0.86 + (0.95)2 = (0.92)3,$$

the lever rule is satisfied. The calibration fits to the Atlantic and Pacific data were made independent of consideration of this rule. Hence, satisfaction of the rule is taken as support for the validity of the model. Furthermore, this lever rule suggests a basin mode hypothesis to explain Cretaceous oceanic anoxia.

6.2. Anoxic case

The present-day global ocean is well-oxygenated. However, the existence of episodes of large-scale anoxia are well-documented in the geologic record. Anoxia occurs whenever the consumption of oxygen exceeds supply. All the model experiments show anoxia occurring as an expansion of the oxygen minimum when v_w reaches or exceeds a critical value. This critical Wyrtki number is a complicated function of both the ventilation number and solubility parameter (ζ).

The results of all the global mode experiments suggest that to sustain a steady-state global anoxia would require an ocean very different from the present. The global fertility experiment suggests that global anoxia with the present-day rate of thermohaline circulation would require the riverine phosphate flux to be almost three times the present value. To have maintained this large riverine phosphate flux for any appreciable length of time in the geologic past seems unlikely.

Neither of the global mode thermohaline circulation rate sensitivity experiments produced anoxic condition with present-day global fertility. Even for the extreme case of a "stagnant global ocean" anoxic conditions did not occur. Eddy diffusion was capable of supplying sufficient oxygen from

the surface to prevent anoxia. Similarly, the global WSBW experiment, with a 50% reduction in the flux of oxygen to the deep ocean, because of reduced oxygen solubility, did not produce a global anoxic ocean. No single hypothesis produced large-scale anoxia which suggests that it is difficult to attain steady-state anoxia on a global scale.

The basin mode provides an explanation for large-scale anoxia that may be particularly appropriate for the Cretaceous. Today, both the Atlantic and Pacific are characterized by Wyrtki numbers <1, far below the critical values for any single experiment. The lever rule suggests a hypothesis for achieving basin-scale anoxia by the net exchange of nutrients from a large to a small basin. The lever rule's weighting of basin Wyrtki numbers by basin area allows a small basin to have a large Wyrtki number while maintaining a global Wyrtki number comparable with the present. This explanation provides an attractive explanation of mid-Cretaceous oceanic anoxic events. The deposition of carbon-rich sediments was most widespread in the North and South Atlantic during that time. These basins were young and much smaller than today. If thermohaline circulation supplied nutrients to these Atlantic basins at the expense of the larger ancient Pacific then a large Atlantic basin Wyrtki number is possible.

Another possible hypothesis to explain the existence of oceanic anoxic events is an analog suggested by the present North Pacific. The oxygen content of mid-depth waters is the lowest and phosphate content the highest of any open ocean values. Possibly, if the new-carbon production were increased locally or the oxygen supplied decreased a tongue of anoxic water would develop in the North Pacific. To quantitatively describe such a tongue would require inclusion of the horizontal balances, i.e. a 2-D model at least. It is interesting that the existence of this low oxygen water is not more evident in mean Pacific oxygen profile which gives the Pacific the appearance characteristic of a well-oxygenated basin.

Another hypothesis for large-scale anoxia is that it is intrinsically a transient phenomena. The marine carbon, oxygen and phosphate system has a built-in negative feedback mechanism. If anoxic conditions develop, the fluxes of carbon and phosphate to the sediment increase. This eventually depletes the nutrient level and ultimately the fertility of the euphotic zone. A decrease in new-carbon production would lead to a decrease in oxygen consumption at depth and the return of well-oxygenated conditions. The carbon, oxygen and phosphate system may exhibit the dynamical behavior of a relaxation oscillation with the Wyrtki number oscillating about the critical value. This explanation is particularly attractive because the geologic record shows rhythmic bedding sediments separated by well-oxygenated biogenic sedimentary sequences [5].

Acknowledgements—Special thanks are due to Klaus Wyrtki for discussions and additional data. We have received considerable assistance from other members of the warm bottom water group including Bill Hay, Eric Barron and Jim Sloan. Thanks are also due to Larry Brand for his helpful discussions.

This paper is a contribution from the Rosenstiel School of Marine and Atmospheric Science. This research was supported in part by National Science Foundation Grant No. OCE 82-15354.

NOMENCLATURE

Depths

(Depths are frequently scaled by α, e.g. αh_2—see Fig. 2 for a sketch of the model domain.)

z = Depth coordinate (positive down, zero at boundary between surface reservoir and deep reservoir)
h = Depth of deep reservoir
h_1 = Depth to top of the anoxic layer
h_2 = Depth to bottom of the anoxic layer
$h_3 = h - h_2$ = Thickness of the bottom oxygenated layer
$h_4 = h_2 - h_1$ = Thickness of the anoxic layer

$\frac{K}{W}$ = Pycnocline scale height

$\frac{\Omega}{v} = \frac{1}{\alpha}$ = Carbon consumption scale height

Dependent variables

C = Particulate organic carbon concentration in deep reservoir
O = Dissolved oxygen concentration in deep reservoir
P = Dissolved inorganic phosphate concentration in deep reservoir

Transport parameters

I = Riverine phosphate flux to surface reservoir
D = Phosphate flux from surface reservoir by deep water formation
F_O = Flux of oxygen to the deep reservoir due to deep water formation
F_P = Flux of phosphate to the deep reservoir due to deep water formation (preformed phosphate)
K = Vertical eddy diffusion coefficient
w = Vertical or upwelling velocity
v = Settling velocity
$T = h/w$ = Residence time

Biological parameters

η = Redfield ratio: ratio of moles of oxygen consumed to moles of carbon dioxide produced by the oxidation of organic material
Ω = Rate constant for the oxidation of particulate organic carbon in the deep reservoir
R = Redfield ratio: ratio of moles of carbon to moles of phosphorus in phytoplankton
$N = vC_0$ = Flux of new-carbon particles out of the surface reservoir
D = Flux of phosphate out of surface reservoir due to deep water formation

Boundary condition parameters

C_0 = Carbon concentration at $z = 0$
O_0 = Oxygen concentration at $z = 0$
P_0 = Phosphate concentration at $z = 0$
O_D = Oxygen concentration in source region
P_{PF} = Phosphate concentration in source region (preformed phosphate)
P_D = Phosphate concentration of the water removed from the surface reservoir ($P_D = P_{PF}$ for global model)
ζ = Ratio of the oxygen concentration in the deep water formation region to O_0
$\xi = P_D/P_0$ = Ratio of the phosphate concentration in water removed from surface reservoir (P_D) to the phosphate concentration at $z = 0$ (P_0)
$\xi' = P_{PF}/P_0$ = Ratio of phosphate concentration in source region (P_{PF}) to phosphate concentration at $z = 0$ (P_0)

Nondimensional numbers

$w_v = \dfrac{w}{\alpha K}$ = The ventilation number

$\nu_w = \dfrac{\eta v C_0}{\alpha K O_0}$ = The Wyrtki number

$\nu_n = \dfrac{vC_0}{\alpha K R P_0}$ = The nutrient number

$(\nu_w)_{crit}$ = The critical Wyrtki number, the Wyrtki number at the onset of anoxia

Other quantities

A_i = The ith coefficient of the oxygen solution
B_i = the ith coefficient of the phosphate solution
$\theta(x) = \begin{cases} 1 & x \geqslant 0 \\ 0 & x \leqslant 0 \end{cases}$ = unit step function where x is an arbitrary argument.

REFERENCES

1. S. O. Schlanger and J. C. Jenkyns, Cretaceous oceanic anoxic events: causes and consequences. *Geologie Mijnb.* **55**, 179–184 (1976).
2. A. G. Fischer and M. A. Arthur, Secular variations in the Pelagic realms. In *Deep Water Carbonate Environments Spec. Publ.* **25**, 19–50 (Edited by H. Cook and P. Enos). Society for Economic Paleontology and Mineralogy (1977).
3. J. Thiede and T. H. van Andel, The paleoenvironment of anaerobic sediments in the Late Mesozoic South Atlantic Ocean. *Earth planet. Sci. Lett.* **33**, 301–309 (1977).
4. T. J. Brawlower and H. R. Thierstein, Low productivity and slow deep-water circulation in mid-Cretaceous oceans. *Geology* **12**, 614–618 (1984).
5. J. Kennett, *Marine Geology*. Prentice-Hall, Englewood Cliffs, N.J. (1982).
6. E. Irving, F. K. North and R. Couillard, Oil, climate and tectonics. *Can. J. Earth Sci.* **11**, 1–17 (1974).
7. H. R. Thierstein, Trends and events in the Mesozoic oceans. In *Proceedings of the Joint Oceanographic Assembly—General Symposia*. Canadian National Committee/Scientific Committee on Ocean (1983).
8. G. W. Brass, J. R. Southam and W. H. Peterson, Warm saline bottom water in the ancient ocean. *Nature* **296** (5858), 620–623 (1982).
9. W. S. Broecker and T. H. Peng, *Tracers in the Sea*. Lamont-Doherty Geological Observatory, Palisades, N.Y. (1982).
10. K. Wyrtki, The oxygen minima in relation to ocean circulation. *Deep Sea Res.* **9**, 11–23 (1962).
11. S. Honjo, S. Manganini and J. Cole, Sedimentation of biogenic matter in the deep sea. *Deep Sea Res.* **29**, 609–625 (1982).
12. S. Levitus, Climatological atlas of the world ocean. *NOAA Prof. Paper 13*. U.S. Printing Office, Washington, D.C. (1982).

13. W. J. Jenkins and J. L. Goldman, Seasonal oxygen cycling and primary productivity in the Sargasso Sea. *J. mar. Res.* **43**, 465–491 (1985).
14. P. N. Froelich, M. L. Bender, N. A. Luedtke, G. R. Heath and T. DeVries, The marine phosphorus cycle. *Am. J. Sci.* **282**, 474–511 (1982).
15. M. Stuiver, P. D. Quay and H. G. Ostlund, Abyssal water carbon-14 distribution and the age of world oceans. *Science* **219**, 849–851 (1983).

APPENDIX

Coefficients Appearing in the Expressions for the Oxygen and Phosphate Profiles

Oxic case

The coefficients appearing in the solutions for the oxygen and phosphate profiles, equations (15) and (16), are

$$A_0 = \frac{\eta v C_0 P_0}{(1 - w_v) K \dfrac{\Omega}{v} O_0} = \frac{v_w}{1 - w_v}, \tag{A.1}$$

$$A_1 = \zeta + \frac{e^{-\alpha h}}{w_v} v_w \tag{A.2}$$

$$A_2 = (1 - \zeta) - \left(\frac{1}{1 - w_v} + \frac{e^{-\alpha h}}{w_v}\right) v_w, \tag{A.3}$$

$$B_0 = -\frac{v_n}{1 - w_v}, \tag{A.4}$$

$$B_1 = \xi - \frac{e^{-\alpha h}}{w_v} v_n \tag{A.5}$$

and

$$B_2 = (1 - \xi) + \left(\frac{1}{1 - w_v} + \frac{e^{-\alpha h}}{w_v}\right) v_n. \tag{A.6}$$

The parameters v_w, v_n and w_v together with scaled depth (α) of the deep reservoir and the boundary condition parameters completely characterize the processes which determine the shapes of the oxygen and phosphate profiles.

Anoxic case

The coefficients A_i appearing in equations (19a–c) for the oxygen profiles are

$$A_0 = \frac{v_w}{1 - w_v}, \tag{A.7}$$

$$A_1 = \frac{v_w \exp(-\alpha h_1)}{w_v}, \tag{A.8}$$

$$A_2 = -\frac{v_w \exp[-(1 - w_v)\alpha h_1]}{w_v(1 - w_v)}, \tag{A.9}$$

$$A_3 = \frac{v_w \exp(-\alpha h_1)}{w_v} \tag{A.10}$$

and

$$A_4 = -\frac{v_w \exp(-\alpha h_1)}{w_v(1 - w_v)}. \tag{A.11}$$

The coefficients B_i appearing in equations (20a–c) for the phosphate profiles are solutions to

$$\begin{bmatrix} 1 & 1 & 0 & 0 & 0 & 0 \\ 1 & \exp(-w_v\alpha_v h_1) & 0 & -1 & 0 & 0 \\ 0 & \exp(-w_v\alpha_v h_1) & 0 & -1 & 0 & 0 \\ 0 & 0 & 1 & \exp(-w_v\alpha h_4) & -1 & -1 \\ 0 & 0 & 0 & \exp(-w_v\alpha h_4) & 0 & -1 \\ 0 & 0 & 0 & 0 & 10 & 0 \end{bmatrix} \times \begin{bmatrix} B_1 \\ B_2 \\ B_3 \\ B_4 \\ B_5 \\ B_6 \end{bmatrix} = \begin{bmatrix} 1 + \dfrac{v_n}{(1 - w_v)} \\ \dfrac{v_n \exp(-\alpha h_1)}{(1 - w_v)} \\ \dfrac{v_n \exp(-\alpha h_1)}{(1 - w_v)} \\ \dfrac{v_n \exp(-\alpha h_1)}{(1 - w_v)} \\ \dfrac{-v_n \exp(\alpha h_1)}{(1 - w_v)} \\ \xi - \dfrac{v_n \exp(-\alpha h_1)\exp(-\alpha h_3)}{w_v} \end{bmatrix}, \tag{A.12}$$

where $h_4 = h_2 - h_1$.